Magnetic Field Swimmer Positioning

Joe Marshall

Abstract— **Several projects have tracked the movement of swimmers in pools using body worn inertial measurement units. In swimming, inertial sensing is subject to large amounts of drift and accumulated error which can only be corrected for after a complete length has been swum. In this article, we present a new method for tracking swimmers by detecting variations in the magnetic field caused by the structure of pools. This method is complementary to inertial positioning, as it allows the direct extraction of position without requiring post-processing, and unlike inertial sensing which loses accuracy over time, magnetic field tracking becomes increasingly accurate towards the end of a length.**

Index Terms—**Magnetic field measurement, Swimming**

I. Introduction

Technology is commonplace in elite swim training and research, most commonly video capture, but also body mounted inertial measurement units (IMUs) [1]–[5], tethering of swimmers to speed detector reels [6] and pools with embedded networks of sensors [7], [8].

Excluding tethered systems, which restrict swimmers' freedom, most systems are essentially non-realtime, in that swimmers swim whilst their performance is recorded and then analysed afterwards.

A few IMU based systems have demonstrated real-time feedback to swimmers of body rotation and arm movement [5], [9], or stroke rate [10]. Using smartphones with inertial sensors, and cheap waterproof cases makes it possible to create systems using commodity hardware for applications such as games which respond to swimming strokes [11].

Most technology is not easily available to non-elite swimmers: Augmented pools are extremely expensive, video recording is not allowed in most pools, tethering is not compatible with shared pool use. IMUs have a major accessibility advantage in two respects, firstly, they are unobtrusive and can easily be used in public pool sessions, and secondly, inertial sensing suitable for sports analysis is widely available in the form of consumer smartphones [12]. However, for real-time feedback to swimmers, IMUs have a major

limitation, which is that the drift that accumulates over time from sensor errors means that they are unable to provide real-time position measurements. It is possible to correct for this once a full length has been swum, and estimate position and velocity [13], [14], but this removes the ability to respond in real-time to a swimmer's movements.

This article presents a drift-free method for determining swimming position in real-time, by sensing variations in magnetic field strength over a swimming pool. The algorithm is evaluated using the sensors of a Google Nexus 4 smartphone. We believe that a combination of this tracking with inertial sensing may provide the basis for a wide range of swimmer aware real-time feedback systems.

The tracking system is evaluated with reference to position measurements taken from synchronised video recordings of swimmers, to demonstrate that it provides a drift free position measurement which is possible to calculate in real time.

II. Magnetic Field Based Positioning

In open outdoor spaces, the Earth's magnetic field is locally constant in direction and magnitude. Indoors however the observed magnetic field will be perturbed by elements of the structure of the building, including steel beams, metal reinforcement in concrete and electrical currents [15], [16].

Whilst these perturbations cause problems for traditional use of a magnetometer for sensing compass direction, the magnetic signature of these disturbances can be detected and used to identify location inside a building. These magnetic disturbances are typically relatively constant over time, meaning that a single magnetic map of a building can be made and used for positioning at later dates [15].

III. Magnetic Field in a Swimming Pool

Lap swimming pools are large rectangular basins, surrounded by reinforced concrete. Steel bars in the reinforced concrete create magnetic field disturbances.

In a lap pool, swimmers typically swim lengths in lanes arranged along the long axis of the pool. Most pools vary in depth along this axis. As such, the perturbation in magnetic field due to the bottom and ends of the pool varies strongly as a person swims along the pool and the distance from the bottom and ends changes. In contrast, the effect of the two sides of the pool is relatively constant, as the swimmer maintains a constant distance and orientation relative to them. Changing lane alters the constant value of the perturbation from the sides, which offsets the profile by a constant value.

Fig. 1(a) shows measurements of the magnitude of magnetic flux density ($|B|$ μ tesla) taken along a single lane in a 25

metre swimming pool by the smartphone used in our experiment, placed flat on the water surface and towed from one end to the other at constant speed. Figure 1(b) shows the same pool 6 months later, in a different lane in the pool, at a faster speed. The magnetic signature does not change over time or lane change, except for a constant offset due to the lane change. Fig. 1(c) and 1(d),1(e) show magnetic signatures of two other pools. The pool in Fig. 1(d) & (e) is interesting, as it shows a different signature when swum in opposite directions. All other pools tested showed the same profile in both directions. We believe this to be due to the movable depth floor of this pool, which uses two lines of scissor jacks beneath the floor. Perturbation of the magnetic field measurement for the vertical line of jacks changes depending on the magnetometer's orientation relative to it, which differs when swimming one direction or the other, unlike orientation relative to bottom of a standard pool.
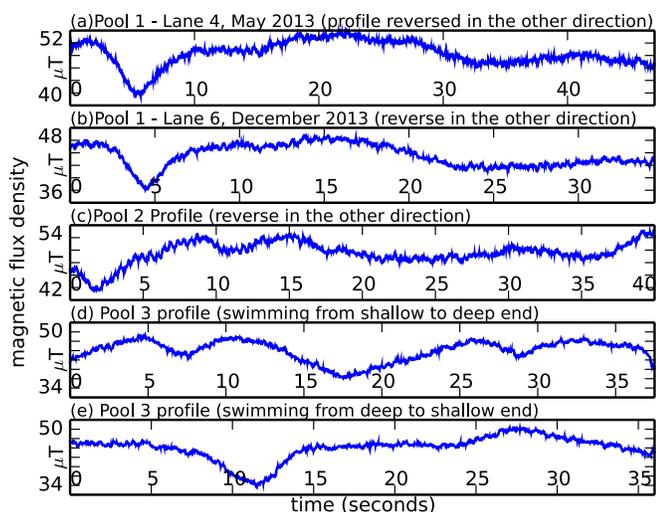
Fig. 1. Magnetic profiles recorded at different pools and times

IV. MEASURING THE MAGNETIC FIELD OF A POOL

A. Sensing Equipment
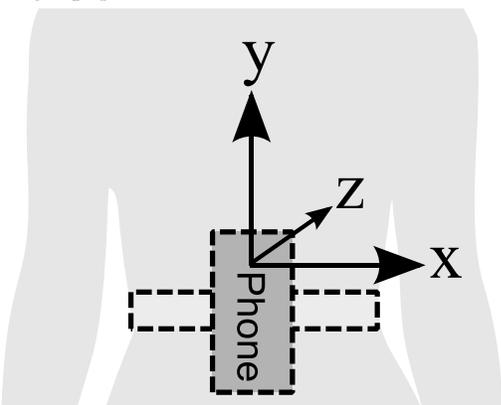
Fig. 2. Placing of the smartphone on the body

A Google Nexus 4 smartphone is placed in a waterproof pouch and strapped tightly onto the central lower back of the swimmer using a simple waist strap and pouch. This position was chosen, as in previous IMU research [1], [3], [5], [13], [14] because it offers a predictable orientation relative to the base of the swimming pool, and allows orientation sensing to reliably detect the direction of swimming. Fig. 2.shows the sensor orientation. Magnetic flux is measured using the built in magnetometer, sampled at 'full speed', nominally 50hz (mean: 48.1hz, s.d. 1.98). The phone contains an Invensys MPU6050 accelerometer & gyroscope with magnetometer input, but no specifications are available for the connected magnetometer (some limited description of the characteristics of Nexus 4 sensors has been extracted by Ma et al. [17]).

B. Recording Magnetic Signature in Real Pool Conditions

The smartphone provides a stable orientation value [17], created using a Kalman filter to fuse accelerometer, gyro and magnetometer sensors. We threshold x-axis (front-back) rotation at 40 degrees to detect when the person starts and stops swimming. 40 degrees was chosen as it is significantly more than the typical maximum backward tilt even in strokes such as breaststroke which involve bringing the head upwards. Orientation is also used to detect laps, by detecting a rotation of 180 degrees around the vertical axis at the end of the pool.

To record the signature of a pool a swimmer swims along the pool on their front while kicking. This keeps the orientation of the sensor constant and provides a constant speed (unlike full stroke swimming which can involve large speed and orientation variations over each stroke). They do this for two lengths, stopping between, to acquire a signature in both directions. We know these were recorded at relatively constant speed and when each length started and ended, so we assume that recorded points are evenly spaced over the length of the pool. This gives us two signatures which vary over distance *d* along the pool, *fwd(d)* and *back(d)*. Unlike indoor navigation projects, which mostly use complete 3 axis signatures (e.g.[18]), we use magnitude of magnetic flux; this is firstly because the major change along the pool is due to the change in depth as the pool base gets further away and only really affects the z axis, so using multiple axes does not add much information , and secondly because using magnitude makes the system more robust to rotation during swimming (pedestrian systems typically assume a relatively constant sensor orientation, which they can calibrate for [15]).

This process has an inaccuracy because at the beginning of a length, the swimmer will push off, which creates a variation in speed at that point. There is less variation at the end of length, as the swimmer touches and comes into the wall whilst bringing their legs down quickly (as an example, we measured three speeds from our video ground truth data, of kicking for 25m length, average speed:0.59m/s, speed from start to 5m: 0.81m/s, speed from 20m to end: 0.53m/s). We correct for this error in a standard pool (which has the same profile in both directions), by creating a final signature from a combination of the second halves of the two signatures. The process for doing this is:

1) Reverse back, to make *back'*. Take the midpoint of *back*.

$$pt_{BACK} = \frac{len}{2}$$

2) Find the point pt_{FWD} in *fwd* which corresponds to pt_{BACK} by minimising the squared difference over a sliding window of length *w = len/4*, vertically offsetting fwd for each possible

value of pt_{FWD} based on the assumption that if pt_{FWD} and pt_{BACK} refer to the same point in the magnetic profile the profile should be equal there (Equation 1). This corrects for the case where a swimmer may swim up in one lane and back in another, so back' will have a constant magnetic offset in comparison to fwd. Equations (1-3) describe this process.

$$vdiff(ofs) = (back'(pt_{BACK}) - fwd(pt_{BACK} + ofs) \quad (1)$$

$$sqdiff(ofs)=$$

$$\sum_{x=pt_{BACK}-\frac{w}{2}}^{x=pt_{BACK}+\frac{w}{2}} \left(back'(x) - fwd(x + ofs) - \text{vdiff(ofs)}\right)^2$$

$$(2)$$

$$pt_{FWD} = pt_{BACK} + \min_{-w<ofs\leq w} sqdiff(ofs) \quad (3)$$

We create a combined signature from the first half of *back'* and the section of *fwd* from pt_{FWD} to the end (Fig. 3). This signature consists only of points where the swimmer was in the more stable second half of each length, so does not include points recorded during initial accelerations of each length.
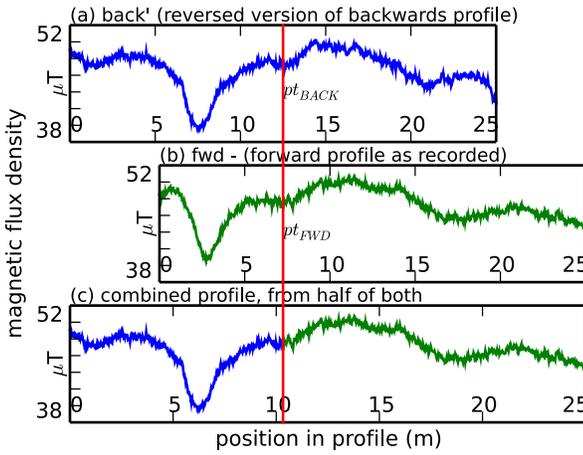
Fig. 3. The acceleration at the start of a length causes the start of the profile to be compressed. The recorded forward and backward magnetic signatures are combined to make a single signature which avoids this inaccuracy.

Fig. 4 shows how the combined profile is not warped by initial acceleration. The dashed line is an example of a profile recorded by swimming (shown smoothed by sliding mean over 1m for clarity), against magnetic points sampled from the same pool using a video based ground truth position.
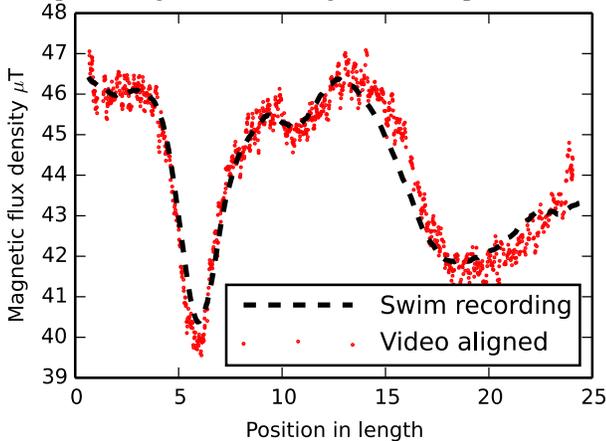
Fig. 4. Swim recorded signature against video aligned magnetic points.

V. Acquiring a Robust Magnetic Signal From a Swimmer During Full Stroke Swimming

Detecting pool position by matching the magnetic signature, requires a high quality magnetic magnitude measurement. To be useful, this must be acquired whilst the swimmer is swimming whatever stroke they desire to perform. Compared to flat swimming, swimming full strokes induces significant noise which requires compensation.

A. Characteristics of swimming induced sensor noise

Magnetometer error caused by reinforcement in concrete is a 'soft iron' error, in that the iron in the reinforcement distorts the earth's magnetic field (in contrast to a 'hard iron' error, where an electric or magnetic component actively generates its own magnetic field) [19]. This causes a magnetometer error that varies depending on the orientation of the magnetometer relative to the source of the error. This error cannot be calibrated for because it is from a source external to the magnetometer [19], further to this, variation in the magnitude of that error is essentially what we are measuring. Because the reinforced concrete grids are essentially planar, and the swimmer is always directly above the floor plane, when swimming flat, the induced error does not change depending on direction in the pool (similarly at either end, the induced error from the end of the pool is constant). In this work, we do not consider other sources of magnetic field perturbations such as electronic devices in the pool area, or the field generated by the smartphone itself, as these are unlikely to be significant as those caused by the large quantity of metal embedded in a typical pool structure.

When collecting the pool signature, swimmers were told to swim flat on their front and kick so their orientation relative to the floor of the pool stays constant. However, when swimming a full stroke, the swimmer may rotate their body away from flat significantly. This is not a problem with breaststroke or butterfly, as angular changes are relatively small. However, when swimming front crawl, there is a significant side to side body rotation, between 40 to 70 degrees from horizontal for a competent swimmer [20]. This causes significant noise as the swimmer rotates, as seen in Fig. 5.
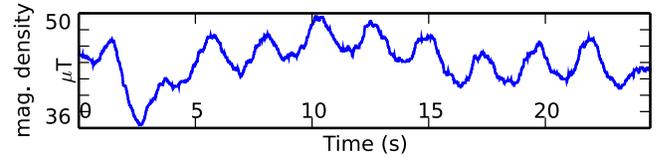
Fig. 5. Side to side rotation causes error in the recorded magnetic signal.

B. Rotation Error Correction

Whilst these errors clearly relate to the sine of the orientation signal, a combination of differing and slightly unpredictable sensor delays on the commodity hardware meant that attempts to create an independent component analysis algorithm for this signal failed. Similarly, whilst the frequency of the swimmer rotation is high compared to the overall changes in magnitude, the irregularity of the rotation meant that low pass filtering did not create a suitably clean signal; low pass filters also created an unacceptable level of

delay for a real time system.

Instead, an adaptive error model is used to correct for these errors, and to create a signal that is close to the reference signal recorded when flat. This model is based on the following assumptions:

1. The output only needs to be a relative magnetic field value, so absolute value is not important. The tracking algorithm is also robust to slight magnitude errors.
2. The error being corrected for is caused by side to side rotations in the stroke, which primarily affect the X and Z axes of the sensor. Whilst all strokes affect the Y axis slightly, we measured typical total rotational ranges of 100-140 degrees side to side swimming crawl, versus approximately 15 degrees front-back in breaststroke and less in crawl.
3. The error is primarily caused by rotation relative to planes (floor, walls), so the axes of any soft iron error will be parallel to the axes of the pool itself.
4. The magnetic field error changes more slowly than the swimming induced error.

In order to error correct for rotation error, the following algorithm is used:

Firstly, take the raw magnetometer magnitude value:

$$mag(t) = \sqrt{M_x(t)^2 + M_y(t)^2 + M_z(t)^2} \ . \qquad (4)$$

This recorded value includes two possible sources of error, soft and hard iron distortions. Hard iron distortions cause a constant offset to be applied for each axis. Soft iron distortions cause the axes to be distorted by an ellipsoid, which in general can be at an arbitrary angle to the axes [19]. Due to Assumption 3, it is possible to assume that the ellipsoid will be axis aligned when the swimmer is flat. Assumption 2 means that we only need to consider effect on X and Z axes.

This means that given correct scaling (s_x, s_y) and offset (o_x, o_y) factors, a normalised version of the recorded magnetic field can be used which will be stable in x/z axis rotation.

$$mnormal(t) = \sqrt{(s_x M_x(t) + o_x)^2 + M_y(t)^2 + (s_z M_z(t) + o_z)^2} \ (5)$$

To calculate these scaling and offset factors, a scoring function $offsetdiff$ is used on a history buffer of magnetic field values to evaluate different factors.

$$offsetdiff(t) = \sum_{i=1}^{t} \big(mnormal(i) - mnormal(i-1)\big)^2$$

$$(6)$$

This function is based on Assumption 4, as it assumes that a better scaling and offset factor will create lower short term variance in the signal. This measure is used rather than a conventional variance to prioritise short-term fluctuation from rotational error over slower underlying field changes.

To optimise scale and offsets, the following algorithm is used:

1. At the beginning of each length, scale and offsets are set to one and zero respectively.
2. As sensor points are received, a circular history buffer 4 seconds long is used to record the full magnetometer vector. Once this buffer contains more than 1 second of data, the scale and offsets are optimised by stepped descent, recalculating the *mnormal* vector for each modification to scale/offset and scoring it using the *offsetdiff* function to find if it is better than the current value. Scales are modified by 0.01 per step, within a range of (-0.95,1.05). Offsets are modified by 0.1 per step, within a range of (-5,5) µT. Up to 10 improvement steps are carried out for each magnetic measurement (at 48.1±1.98hz as above).

Scale and offset factors are reset on a per length basis. This is because in practice the correct factor will change significantly over multiple lengths, even between two lengths in the same direction, it is hypothesised that this may be due to changes in equipment temperature due to uneven temperature in the water or sensors warming up, sensor attempts at automatically calibrating, which fail in such high magnetic error surroundings, changes in sensor orientation due to slight posture changes, or other un-modelled factors.

Fig. 6 shows an example result from this optimisation.
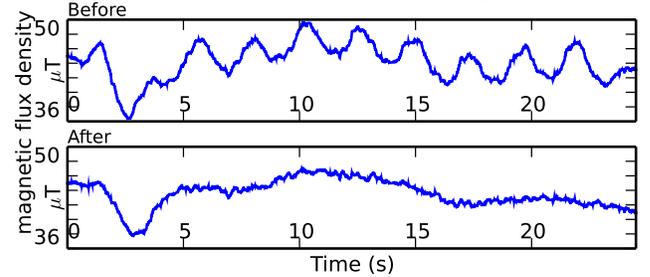
Fig. 6. Recorded magnetic signal with rotation induced noise removed.

VI. MAGNETIC SIGNATURE TRACKING

The magnetic tracking algorithm uses as input the error corrected magnetic history for the current length. This is matched against the signature to acquire position at 0.1m resolution once per 10 magnetometer points (i.e. at 5HZ).

The algorithm used is a dynamic programming algorithm in which at each timestep the recent history of sensed magnetic field strength is compared against areas of the magnetic signature which it plausibly could represent, with plausibility defined by the output of previous time steps and constraints on how fast swimmers can realistically move. It is inspired by Dixon's on-line dynamic time warping algorithm [21], but uses a regional matching window for each point, and ongoing cost is simplified to simply a true/false plausibility vector.

A. Generation of Signature Matrix
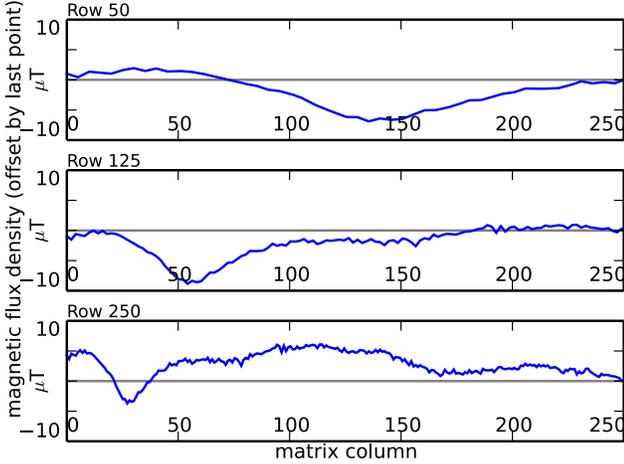
Fig. 7. Each row in the signature matrix contains a subset of the full pool signature (row 250). Each row is offset so the last value in the row is zero.

When the pool signature is captured, the system generates a signature matrix *SM* of fixed dimensions 249x250 using (7) below (where *len* is the full length of the recorded signature, the implementation uses linear interpolation for intermediate values of the signature vector),

$$SM(r,d) = \text{signature}\left(d \times \frac{r}{250}\right) - \text{signature}\left(len \times \frac{r}{250}\right) \quad (7)$$

Each line of the matrix takes a subset of the complete pool signature from the start to a proportion of the way along the pool (Fig. 7), and offsets values by the last value in that row, so that it always ends with a zero. 250 points are used to acquire 10cm accuracy in a standard 25 metre pool. 249 rows are used to avoid template rows generated from a single point.

Matrix generation is done once per pool signature recording, so is not performance critical. Generation of the signature matrix allows for fast matching of recorded magnetic data against all possible positions in the pool profile using vector & matrix operations.

B. Per Length Initialisation

At the beginning of a length, a plausibility vector is initialised; this is a Boolean vector of length 249, initially set to true for all points. The plausibility vector is true for points which it is plausible that the person may be at in the current time step. The initial time step occurs at 0.4 seconds from the detection of swimming starting, when 3 points of history data have been collected.

C. Per frame tracking

TABLE I
DEFINITION OF VARIABLES AND CONSTANTS

Name	Description
sigsteps=10	Number of signature steps per metre
$s_{min} = 0.25 \times$ sigsteps	Minimum speed (signature steps per second)
$s_{max} = 3 \times$ sigsteps	Maximum speed (signature steps per second)
dt	Time step since last frame (seconds)
t	Time since beginning of length (seconds)
PLB_t	Plausibility vector at time t before tracking (Boolean vector)
PBA_t	Plausibility vector at time t after tracking
len	Number of points in magnetic history vector

The algorithm assumes a minimum and maximum swimming speed of 0.25 m/s and 3 m/s respectively, chosen to range from extremely slow to well above world record speed. Table I shows the variables and constants used.

1) Update plausibility vector

At each time step, the plausibility vector is updated using Equation (10) below. This takes account of both the minimum and maximum swimming speeds, and the points which were marked as plausible in the previous time step and is constructed as follows:

To update the plausibility vector for a time step, for each position to be a plausible result in this time step, it must satisfy two constraints:

Global speed constraint: Is it possible that someone could start a length at the time they started and have got to this point by the current time?:

$$\text{plaus}_{\text{global}}(x) = (t * s_{min} < x < t \times s_{max}). \quad (8)$$

Local speed constraint: There must be a point in the previous time step plausibility vector that this point could be reached from by travelling at a speed between s_{min} and s_{max}:

$$\text{plaus}_{\text{local}}(x) =$$
$$\exists\, k: \left(dt * s_{min} < k < dt * s_{max} \ \wedge \text{PLA}_{t-1}(x - k)\right). \quad (9)$$

The final plausibility value is a simple AND operation on these two boolean functions:

$$\text{PLB}_t(x) = \text{plaus}_{\text{global}}(x) \wedge \text{plaus}_{\text{local}}(x). \quad (10)$$

2) Normalise History Vector

For each tracking frame, the magnetic history for the length swum so far is taken, resized to length 250, and offset by the final value (11), so that it is in the same form as the rows in the magnetic signature matrix. Again, linear interpolation is used for intermediate history values.

$$histnorm(x) = history\left(x \times \frac{len}{250}\right) - history(len) \quad (11)$$

3) Score Plausible Rows

The last 4 seconds of the history vector are then compared against the relevant section of every row in the signature matrix for which the plausibility vector PLB is true. The comparison uses a simple sum of squared differences (12).

$$timeOfs = \frac{4*250}{t}$$
$$sqdiff(x) = \sum_{k=250-timeOfs}^{250}[histnorm(k) - SM(x,k)]^2 \quad (12)$$

4) Output Tracking Position

The final output position is the one with the lowest squared difference to the signature array.

$$outposition = minpos_{x \in PLB_t}(sqdiff(x)) \quad (13)$$

5) Update Plausibility Vector

The minimum value for *sqdiff* is found, and a plausibility threshold is set as 5.0 × minimum value. The plausibility vector after the time step (PLA) is set based on this threshold.

$$minVal = \min_x scorefn(x) \quad (14)$$
$$plausibleMax = 5.0 * minVal \quad (15)$$
$$\text{PLA}_t(x) = \text{PLB}_t(x) \wedge (scorefn(x) \leq plausibleMax) \quad (16)$$

VII. ALGORITHM EFFICIENCY

A. Rotation Error Correction

The rotation error correction uses a magnetic history buffer containing 200 samples (4 seconds at 50hz). As each sample comes in, up to 10 optimisation steps occur. These require:

1) Calculate the magnitude of each point with offsets to X and Z (5 additions, 5 multiplications, 1 square root per point)
2) Calculate the offset difference function (1 subtraction, 1 multiplication per point)

This gives a total of $200 \times 13 \times 10 = 26,000$ floating point operations per optimisation step, or $1,300,000$ per second, all of which are trivially parallelisable and vectorisable.

B. Signature Tracking

Without the local plausibility vector constraint, the worst case scenario is that the algorithm will require searching the full range between the fastest and slowest possible positions as defined by the global minimum and maximum speeds, defined by (17) below. Further to this, the scoring algorithm uses a 4 second window, which means it only compares against selected columns of the signature matrix after 4 seconds has elapsed. The number of columns compared is defined by (18).

$$rowrange(t) = \min(250, t \times s_{max}) - \min(250, t \times s_{min}) \quad (17)$$

$$columnrange(t) = \begin{cases} 250 & t \le 4 \\ \left(\frac{4}{t}\right) * 250 & t > 4 \end{cases} \quad (18)$$

The number of comparisons between values required at a given time is equal to the product of $rowrange(t)$ and $columnrange(t)$. For our maximum and minimum values, matrix size and time step, taking a maximum of this product means that the maximum number of comparisons is 27777, which given the relatively simple calculations involved (one floating point subtraction, one multiplication and one addition per comparison) is easily within the capabilities of even low end smartphones (e.g. The author's Sony Xperia M reports a real world throughput of $1,009,000,000$ floating point operations for multiplication of large double precision floating point matrices). The scoring operations are also trivially parallelisable and well suited to vector operations.

The number of comparisons in the worst case grows as the square of the signature matrix resolution, meaning that the balance between resolution and performance must be carefully considered. It should be noted that the magnetic signal does not change very quickly, so 250 points is easily able to capture the full range of variation in all the pools tested.

Whilst as described above, the worst case scenario is well within the capability of modern mobile hardware, in practice, the local constraint in the plausibility vector improves the performance considerably, vastly reducing the search space. As an example, Fig. 8 shows one length of tracking, with the received magnetic signal on the bottom, the target signature on the right, and the detected position of the magnetic tracker as each measurement is received shown as the central black line. The grey channel around the central measurement shows the range of plausible values as each measurement comes in, typically 10-20 possible positions are tested (2500-5000 comparisons), with a worst case of approximately 50 (up to 12500 calculations).

C. Overall Algorithm Efficiency

As shown above, in the worst case, the algorithm shown

here requires 1,327,000 floating point calculations per second, making it easily within the range of a standard smartphone level processor such as the 1Ghz ARM7 core used in the author's Sony Xperia m. A majority of the time currently is spent performing rotational noise reduction; in future we believe it may be possible to reduce this by designing an algorithm to perform the error reduction at 5hz, in tandem with the tracking algorithm, to allow this algorithm to be implemented on simpler wearable sensor hardware.
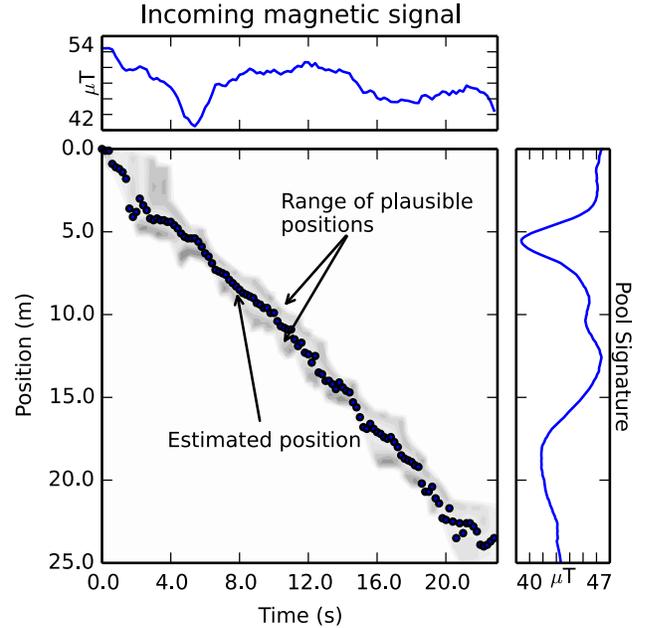
Fig. 8. A plot of a tracking result, showing the estimated position, and the range of positions which are plausible position estimates for each time step.

VIII. ACCURACY EVALUATION

To evaluate the accuracy of the algorithm, a test was run with 3 swimmers, in a standard 25 metre public pool. Each swum 2 lengths kicking, then continued to swim front crawl. 1 participant unfortunately managed to loosen the strap of the phone holder during their swim, which meant that their data was lost. A total of 10 lengths were recorded from the remaining two participants. Front crawl was chosen as being the stroke with the greatest amount of rotation induced noise in the signal. Swimmers were both male intermediate swimmers (swimming at a pace of 6 or 7 minutes per 400m). The swimmers varied their speed during the testing, between 0.63 m/s to 1.14 m/s average speed per length. One participant swam parts of their lengths doing *catch-up drill*, where the swimmer uses exaggerated, slower stroke actions.

A pool profile recorded from kicking lengths of one participant was used for all testing, to provide support for the idea that the profile is unique to the pool rather than the swimmer. This did not alter the results in comparison with using the swimmer's own recorded profile.

A. Video Based Ground Truth
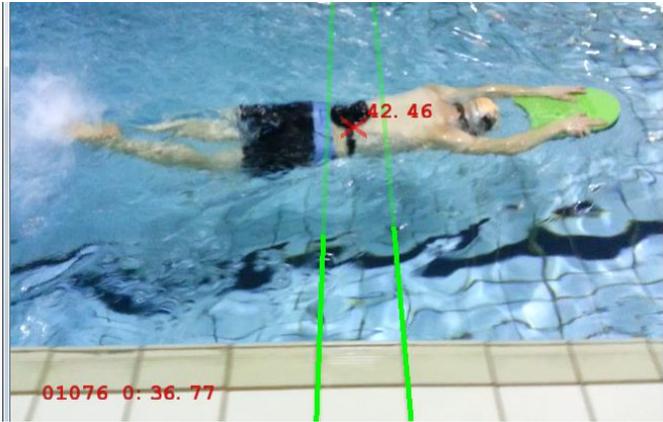
Fig. 9. A suitable ground truth dataset was acquired with reference to the regular 250mm spaced (240mm + grouting) tiling on the side of the pool.

To acquire a ground truth dataset, the swimming was video recorded. The pool used is uniformly tiled along the edge, with the pool edge being level to the water. Regular reference points on this tiling were used to create a ground truth position in the pool, by hand annotating features on the image and using a simple planar homography to measure the position in the pool of the belt on which the system was mounted (Fig. 9). This gave a ground truth measurement that is accurate to more than the 10cm resolution that the tracking algorithm works at. Overall, 5265 ground truth data points were recorded, along the full pool length for all lengths swum.

B. Accuracy Measurements

TABLE II
DESCRIPTIVE STATISTICS FOR MAGNETIC TRACKING ACCURACY

Statistic	Value
Absolute error mean	$\mu_{abserror}=0.73$m
Abs. error standard deviation	$\sigma_{abserror}=0.65$m
Correlation with ground truth	$r^2=0.98$
error mean	$\mu_{error}=0.02$m
error standard deviation	$\sigma_{error}=0.98$m

Fig. 10(a) shows a plot of magnetic measurements versus ground truth measurements. The mean absolute error over the dataset is 0.73m. Fig. 10(b) shows the distribution of the error; 71.5% of points are within ±1 metre of the ground truth data. This exceeds the performance of standard person worn magnetic tracking algorithms e.g. [15], [18], in part due to swimming specific constraints on initial position, velocity and orientation. The fact that swimming pools are strongly directional in their construction is also likely to be a factor, in that the magnetic field is not subject to large variation as a swimmer moves from side to side in the pool, in contrast to the building structure induced errors described by [15].

As can been seen from the diagrams, the correlation between the two is extremely strong (r^2=0.98), Fig 10(c) shows a Bland-Altman plot [22] which demonstrates the algorithm performance through the length, showing that it actually improves in accuracy towards the end. Table III shows descriptive statistics relating to this improvement. This improvement is in contrast to inertial sensor based systems, which whilst they can be accurate at the beginning of a length,

due to drift caused by noise in the sensors become increasingly poor over time [13]. For this reason, inertial positioning systems for swimming cannot be real-time and need to apply correction algorithms to the inertial data at the end of a length when the swimmer is at a known position.
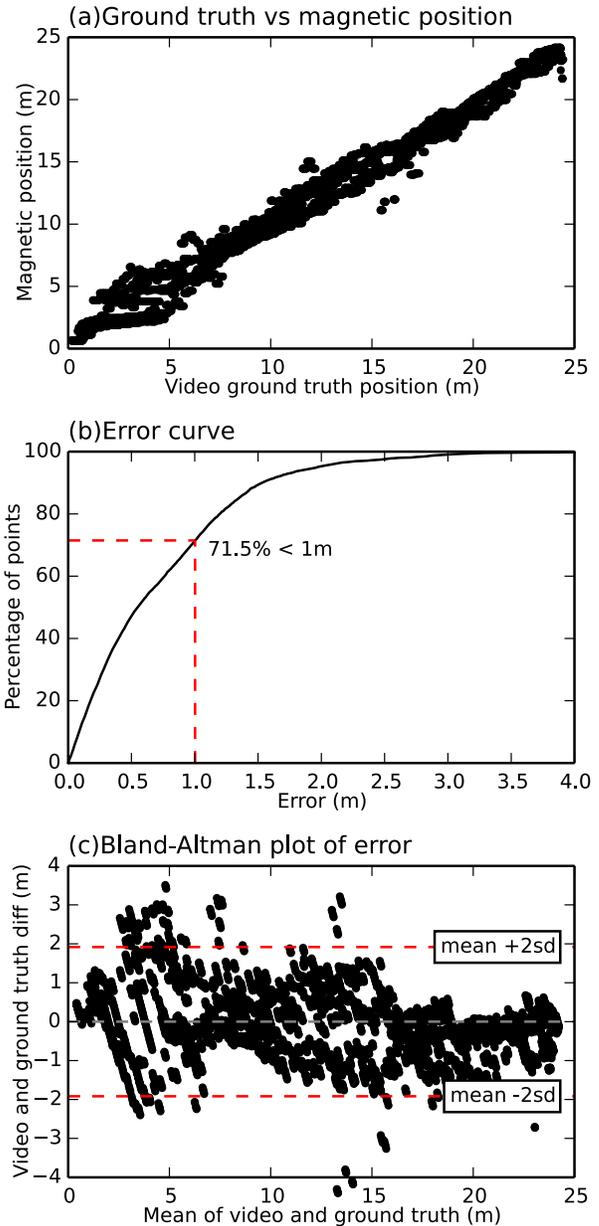
Fig. 10. Performance of the algorithm against ground truth measurement

TABLE III
PERFORMANCE AT DIFFERENT POINTS IN THE POOL

Range from	Range to	$\mu_{abserror}$	$\sigma_{abserror}$
0	5	1.11	0.81
5	10	0.63	0.58
10	15	0.84	0.50
15	20	0.66	0.70
20	25	0.47	0.47

IX. Algorithm Characteristics and Application

A. Potential for Combination with Inertial Tracking

TABLE IV
COMPARISON OF MAGNETIC AND INERTIAL TRACKING

	Magnetic Tracking	IMU Tracking
Resolution	Low (10cm)	High (<1cm)
Output position	Absolute position	Position relative to last known point
Change in position error over time	Error stable or decreasing	Begins low then increases (drift)
Frequency	Low (5hz)	High (100-1000hz)
Posture Tracking	None	Can estimate body position

Table IV summarises characteristics of the magnetic tracking algorithm described in this paper, contrasted against inertial sensor based real-time tracking. It is clear that this algorithm has potential for combination with an inertial sensing algorithm in order to create a high-resolution, low drift estimate of swimmer position and velocity. Magnetic sensing is also advantageous compared to IMU systems which adapt each length, such as [1], in that it is entirely per length, and does not assume that participants will be swimming in a similar manner for all lengths; this is particularly important for less expert swimmers, who may be swimming irregularly, but also potentially affects those who may be doing a lot of *drill swimming*, where swimmers perform movements designed to break down a small element of the act of swimming. These significantly change the dynamics of the swimming action, in a way that could potentially hinder adaptive inertial systems as the way a person swims can change entirely on every length.

B. Potential Applications

Ongoing and future work involves creating real-time audio, visual and vibro-tactile feedback systems for swimming. For these systems, knowing where in the pool a swimmer is is important. For example if a system is aiming to aid swimmers with a tumble turn, knowing that the swimmer is nearing the end of the pool could allow the system to create relevant feedback to the user, firstly to suggest breathing early, before they need to turn, then to aid them in initiating their turn, and finally to evaluate the movements of their turn. Our experiments with inertial sensors suggest that drift in integration during a length of swimming is too much for even such simple cueing to be practical with an inertial solution, as cuing may happen significantly too early or late.

REFERENCES

[1] T. Le Sage, A. Bindel, and P. Conway, "Kalman filter design for application to an INS analysing swimmer performance," in *18th European Signal Processing Conference. EURASIP 2010.*, 2010, pp. 1723–1727.
[2] N. Davey, M. Anderson, and D. A. James, "Validation trial of an accelerometer-based sensor platform for swimming," *Sport Technol*, vol. 1, no. 4–5, pp. 202–207, Dec. 2008.
[3] P. Siirtola, P. Laurinen, J. Roning, and H. Kinnunen, "Efficient accelerometer-based swimming exercise tracking," in *2011 IEEE Symposium on Computational Intelligence and Data Mining (CIDM)*, 2011, pp. 156–161.
[4] A. Stamm, D. V. Thiel, B. Burkett, and D. A. James, "Towards determining absolute velocity of freestyle swimming using 3-axis accelerometers," *Procedia Eng*, vol. 13, pp. 120–125, 2011.
[5] M. Bächlin and G. Tröster, "Swimming performance and technique evaluation with wearable acceleration sensors," *Pervasive Mob Comput*, vol. 8, no. 1, pp. 68–81, Feb. 2012.
[6] T. Pedersen and P. Kjendlie, "The effect of the breathing action on velocity in front crawl sprinting," *Port J Sport Sci*, vol. 6, no. 2, pp. 75–77, 2006.
[7] T. Le Sage, A. Bindel, P. Conway, S. Slawson, and A. West, "Development of a wireless sensor network for embedded monitoring of human motion in a Harsh environment," in *2011 IEEE 3rd International Conference on Communication Software and Networks*, 2011, pp. 112–115.
[8] H. M. Toussaint, A. Beelen, A. Rodenburg, A. J. Sargeant, G. de Groot, A. P. Hollander, and G. J. van Ingen Schenau, "Propelling efficiency of front-crawl swimming," *J Appl Physiol*, vol. 65, no. 6, pp. 2506–2512, Dec. 1988.
[9] R. M. Hagem, D. V. Thiel, S. G. O'Keefe, N. Dahm, A. Stamm, and T. Fickenscher, "Smart optical wireless sensor for real time swimmers feedback," in *IEEE Sensors*, 2012, pp. 1–4.
[10] R. M. Hagem, S. G. O'Keefe, T. Fickenscher, and D. V. Thiel, "Self Contained Adaptable Optical Wireless Communications System for Stroke Rate During Swimming," *IEEE Sens J*, vol. 13, no. 8, pp. 3144–3151, Aug. 2013.
[11] H. Lee, M. Moon, T. Park, I. Hwang, U. Lee, and J. Song, "Dungeons & swimmers," in *Proceedings of the 2013 ACM conference on Pervasive and ubiquitous computing adjunct publication - UbiComp '13 Adjunct*, 2013, p. 287.
[12] M. W. McCarthy, D. A. James, and D. D. Rowlands, "Smartphones: Feasibility for Real-time Sports Monitoring," *Procedia Eng*, vol. 60, pp. 409–414, Jan. 2013.
[13] F. Dadashi, F. Crettenand, G. P. Millet, and K. Aminian, "Front-crawl instantaneous velocity estimation using a wearable inertial measurement unit.," *Sensors (Basel)*, vol. 12, no. 10, pp. 12927–39, Jan. 2012.
[14] A. Stamm, D. A. James, and D. V. Thiel, "Velocity profiling using inertial sensors for freestyle swimming," *Sport Eng*, vol. 16, no. 1, pp. 1–11, Dec. 2012.
[15] J. Haverinen and A. Kemppainen, "Global indoor self-localization based on the ambient magnetic field," *Rob Auton Syst*, vol. 57, no. 10, pp. 1028–1035, 2009.
[16] M. Angermann, M. Frassl, M. Doniec, B. J. Julian, and P. Robertson, "Characterization of the indoor magnetic field for applications in Localization and Mapping," in *2012 International Conference on Indoor Positioning and Indoor Navigation (IPIN)*, 2012, pp. 1–9.
[17] Z. Ma, Y. Qiao, B. Lee, and E. Fallon, "Experimental evaluation of mobile phone sensors," in *24th IET Irish Signals and Systems Conference (ISSC 2013)*, 2013, pp. 49–49.
[18] J. Chung, M. Donahoe, C. Schmandt, I.-J. Kim, P. Razavai, and M. Wiseman, "Indoor location sensing using geo-magnetism," in *Proceedings of the 9th international conference on Mobile systems, applications, and services - MobiSys '11*, 2011, p. 141.
[19] M. Garton, A. Wutka, and A. Leuzinger, "Local Magnetic Distortion Effects on 3-Axis Compassing," *PNI Sens Corp Tech Reports*, 2009.
[20] C. J. Payton, R. M. Bartlett, V. Baltzopoulos, and R. Coombs, "Upper extremity kinematics and body roll during preferred-side breathing and breath-holding front crawl swimming.," *J Sports Sci*, vol. 17, no. 9, pp. 689–96, Sep. 1999.
[21] S. Dixon, "An on-line time warping algorithm for tracking musical performances," in *IJCAI'05 Proceedings of the 19th international joint conference on Artificial intelligence*, 2005, pp. 1727–1728.
    J. M. Bland and D. Altman, "Statistical methods for assessing agreement between two methods of clinical measurement," *Lancet*, 1986.

Joe Marshall received the B.A. in Computer Science from Cambridge University, UK in 2000 and a Ph.D. from the University of Nottingham, UK in 2008.

From 2008 to the present, he has worked as a Research Fellow at the Mixed Reality Lab at the University of Nottingham. His research interests centre around the development and study of technology for sports, games and artistic performance, with a focus on mobile devices.

Mr Marshall is the holder of an Early Career Fellowship from the Leverhulme Trust.